

SEISMIC ANALYSIS OF CONCRETE ARCH DAMS BY SMEARED CRACK APPROACH

Radin ESPANDAR¹, Vahid LOTFI² And Ghani RAZAQPUR³

SUMMARY

A smeared crack approach is used in a 3D finite element model of an arch dam to analyze its seismic response. The crack-induced nonlinear behavior of Shahid Rajaei arch dam in Iran, subjected to the Friuli-Tolmezzo earthquake, is compared to its linear elastic behavior under the same excitation. It is concluded that the dam will crack extensively and stress redistribution will occur. However, the maximum compressive stresses and displacements will not be significantly affected by cracking.

INTRODUCTION

Determining the seismic behavior of concrete arch dams is a complex task. The main reasons are the nonlinear behavior of the dam body and the fluid-structure and soil-structure interactions. The nonlinearity is mainly due to the low tensile strength of weak planes, such as vertical contraction joints, horizontal working joints, and dam-foundation interface [5,8,10]. However, cracking at other locations and non-predefined directions in the mass concrete is also probable and potentially important.

In most cases of the previous works, nonlinearity has been accounted by utilizing nonlinear interface elements or the elasto-plastic models for concrete [8,9]. In this paper, a finite element program, called SNAP [6], is developed, based on a smeared crack approach to investigate concrete nonlinearity and its effect on the response of arch dams. The model captures crack initiation by applying a bilinear softening rule based on fracture energy release equivalence criterion, similar to the works of de Borst et al. [2] and Rots[11].

MATERIAL MODEL

In the present study, the 3D formulation begins by decomposing the incremental strains $\{\Delta\epsilon\}$ into the uncracked concrete strains $\{\Delta\epsilon^{co}\}$ and the crack strains $\{\Delta\epsilon^{cr}\}$:

$$\{\Delta\epsilon\} = \{\Delta\epsilon^{co}\} + \{\Delta\epsilon^{cr}\} \quad (1)$$

In the pre-cracked state, for simplicity a linearly elastic stress-strain relationship for concrete is assumed. For the cracked concrete, a strain softening model is adopted, which relates the surface tractions to the equivalent crack strain through a tangent matrix, viz.

$$[D^{cr}] = \begin{bmatrix} D_c & 0 & 0 \\ 0 & \beta_c G & 0 \\ 0 & 0 & \beta_c G \end{bmatrix} \quad (2)$$

¹ Ph.D. Candidate, Civil Eng. Dept., Amirkabir Univ., Tehran, Iran, & Research Associate, Carleton Univ., Ottawa, Canada.

² Assistant Professor, Civil Engineering Department, Amirkabir University, Tehran, Iran.

³ Professor, Civil and Environmental Engineering Department, Carleton University, Ottawa, Canada.

The properties of the cracked concrete constitutive matrix, $[D^{cr}]$, forms the crux of the smeared crack formulation. Normally, it is assumed that there is no interaction between modes I and II of failure, thus, the coupling between the normal and shear components in the crack traction-strain expression is neglected [11]. In eq. (2) β_c is assumed to be a constant, referred to as the shear retention factor (here assumed as $\frac{1}{9}$), G is the usual uncracked concrete shear modulus, and D_c is the cracked concrete modulus, normal to the crack plane defined as follows:

$$D_c = -\frac{f_t^2 l^*}{2\alpha_2 G_f} \quad (3)$$

in which f_t and G_f are the concrete tensile strength, or crack initiation stress, and fracture energy release rate, respectively. The factor α_2 is varies which is different for each region of the softening curve, i.e. it changes in the second segment of this curve which starts at a reduced tensile strength of $f_t^* = \alpha_1 f_t$ (Fig. 1). In this study, the values of 0.01 for α_1 and 1.0, 0.001 for α_2 in the two regions of softening branch are used, respectively. l^* is the crack bandwidth, and in finite element analysis to overcome lack of objectivity with respect to the mesh size [1], this is taken as a characteristic length. In the current study, the characteristic length is chosen as the side of an equivalent cube having the same volume as the tributary volume at the crack sampling point in a 20-node solid isoparametric element [3].

Following the details given elsewhere [7], the incremental stress-strain relation at a crack sampling point can be written as:

$$\{\Delta\sigma\} = ([D^{co}] - [D^{co}][T_\epsilon^*]([D^{cr}] + [T_\epsilon^*]^T[D]^{co}[T_\epsilon^*])^{-1}[T_\epsilon^*]^T[D^{co}])\{\Delta\epsilon\} \quad (4)$$

in which $\{\Delta\sigma\}$ is the incremental stress vector, $[D^{co}]$ is the elastic constitutive matrix of intact concrete, and $[T_\epsilon^*]$ is a 6×3 matrix transforming increments of crack strains from local to global system of coordinates. This is obtained by selecting the appropriate columns of the usual transformation matrix $[T_\epsilon]$.

NONLINEAR SEISMIC ANALYSIS OF SHAHID RAJAEI ARCH DAM

Consider the idealized symmetric model of Shahid Rajaei concrete arch dam in Fig. 2. This is a dam with a height of 130 m and crest length of 420 m. The dam is located in north of Iran, in the seismically active foothills of Alborz Mountains near the city of Sari. The dam's seismic response is analyzed using a linear and a nonlinear approach.

Let case L designate a linear analysis, used mainly for comparative purposes, while case SM denotes a nonlinear analysis by the proposed smeared crack model. In both cases, the same finite element discretization is used, which consists of 487 nodes and 76 isoparametric 20-node solid elements in two layers through the thickness of the dam. The earthquake excitations include two components of the Friuli-Tolmezzo earthquake (the cross-canyon component is neglected) whose record is normalized based on the frequency content for MDE condition with the peak ground acceleration of 0.42g. The Rayleigh damping coefficients were determined such that equivalent damping for frequencies close to the first and sixth modes of vibration would be 12% of the critical damping.

Table 1: Maximum displacements at dam crest

Case	Component	Displacements of Dam Crest (mm)		
		Left Quarter Point	Center Point	Right Quarter Point
L (Linear)	U (Cross Canyon)	26	0.0	-26
	V(Stream)	61	105	61
	W(Vertical)	-5	-12	-5
SM (Smeared Crack)	U (Cross Canyon)	23	0.0	-23
	V(Stream)	59	92	59
	W(Vertical)	5.6	16	5.6

As for foundation, it is assumed rigid to keep the computational time realistic. Although this assumption would drastically influence the boundary stresses in the case L, it is believed to be less important for the case SM due to cracking of elements located at boundaries. In addition, the assumption of rigid foundation has less effect on the stresses near the spillway, where the major mode of failure is expected to occur. In the current analysis, the dam-water interaction effects are included by the conservative but computationally efficient modified Westergaard method [4]. In this approach, consistent added mass matrices are introduced which can be easily combined with the mass of the dam body.

Although different concrete mixes were used in the dam construction, the material properties are assumed uniform. For this study, they are: $E = 30.0$ GPa, $\rho = 2400$ kg/m³, $\nu = 0.18$, $f_t = 1.5$ MPa, and $G_f = 600$ N/m. It is noted that the tensile strength is chosen to be more representative of the strength at planes of weaknesses (contraction joints or dam-foundation interface). This is important for a realistic simulation since in the present analysis we are not using discrete crack elements to model these weak planes.

The analysis was commenced by applying static loads. These include the dead weight of the dam body and the hydrostatic water pressures corresponding to 122 m height of reservoir water. These loads were incrementally increased in time until they reached their full magnitude. A time step of $\Delta t = 0.005$ sec was selected for time integration. In this respect, the dead load is applied in two increments and the hydrostatic water pressures thereafter in eighteen increments at negative range of time. At time zero, the actual nonlinear dynamic analysis starts with the static displacements and stresses being applied as initial conditions.

To study the displacements of the dam, three nodes are selected on the dam crest. These are located at the center, and at approximately the left and the right quarter points. The maximum displacements through time for each of the x, y, and z directions at these nodes are summarized in Table-1, i.e. U, V, and W, respectively. Note that positive displacement is assumed in downstream direction. Observe the expected symmetry of the displacements in the table. In Fig. 3 and 4 for the same points, displacement histories in the stream direction are compared for the linear and the nonlinear cases. It is apparent that the displacements are very close for the two models while the maximum values of displacements are slightly higher for the linear model, except for the vertical components. This is a result of increased damping due to the nonlinear response of the dam. Meanwhile, in the first large excursion of the central point of the dam crest, which occurred at 4.45 sec, compared with the linear model the vibration period lengthened about 13% to 0.54 sec.

Table 2: Maximum tensile and compressive stresses

Case	Location	Maximum Principal		Minimum Principal	
		Stress σ_1 (MPa)		Stress σ_3 (MPa)	
		Upstream	Downstream	Upstream	Downstream
L (Linear)	Spillway	5.90	6.70	-13.77	-13.77
	Base and Abutments	14.74	0.28	-6.23	-10.00
SM (Smearred Crack)	Spillway	5.68	4.13	-13.80	-11.54
	Base and Abutments	1.96	1.50	-4.77	-9.29

The results of the envelope of maximum principal stresses throughout the analysis period are obtained and they are summarized in Table-2 while the tensile stress envelopes are displayed in Figs. 5-8.

In the linear analysis, very high tensile stresses are calculated at the base of the dam (Fig. 5), which are due to the rigid foundation model assumption. Furthermore, high tensile stresses occur in the area of spillway, which in reality are released with opening of the contraction joints. A maximum compressive stress of 13.77 MPa is calculated in the upstream face near the spillway region. (Fig. 6).

For the smeared crack model, high tensile stresses at the base of the dam are detected and compared against the corresponding linear model results (Figs. 7-9). As stated earlier, high tensile stresses develop in this region in the linear case. However, these stresses are limited to 1.50 MPa for the nonlinear case (Fig. 9), i.e. to the tensile strength of concrete, and then they decrease significantly due to softening after crack formation in this region. It is also noticed that later ($t = 4$ seconds), tensile stresses increase again in a direction different from the previous crack direction and reach a maximum value of 1.8 MPa for a typical stress sampling point. Overall, high tensile stresses at the base and abutments are totally limited to 1.96 MPa by the help of cracks forming in these regions

(Figs. 7,8). In the spillway region, even though cracks and attendant softening are modeled, still relatively high tensile stresses occur in the upstream face (5.68 MPa compared to 5.90 MPa in the Linear Case). This is mainly due to the deficiency of the fixed single crack model and possibilities of high tensile stresses in both the arch and the cantilever directions in this region. On the other hand, the maximum compressive stress in the spillway region is -13.80 MPa (Figs. 10,11), which is approximately the same as predicted amounts by the linear model.

The extent of softening obtained from the different regions of the smeared crack model is very clear from the graphs of reduced tensile strength (Figs. 12,13) at the end of the earthquake excitation duration, i.e. $t = 6.0$ sec. These figures, together with the crack patterns (Figs. 14,15) clearly illustrate the extent of damage occurring in the dam body. It is noticed that in the upstream face, cracks are formed near the base, abutments and spillway regions. Meanwhile, a major part of the downstream face of the dam is also cracked.

CONCLUSIONS

A computer program is developed for the crack-induced nonlinear seismic analysis of concrete arch dams using the smeared crack model of concrete. An idealized symmetric model of Shahid Rajaee arch dam is considered and two cases are analyzed, linear model (Case L), and nonlinear smeared crack model (Case SM). The main conclusions of the analysis are:

- Calculated displacements by the models are very close to each other. The maximum values of displacements are slightly higher for the linear model with the exception of the vertical components, which are smaller.
- Both models yield the same states of stress and deformation at the end of self-weight analysis.
- At the end of static analysis, high tensile stresses are observed in the linear case at the upstream face of the dam base. For the smeared crack model after crack formation, the tensile stresses decrease significantly due to strain softening. However, close to the end of analysis, in this region tensile stresses increase again in a direction different from the initial crack direction and reach a maximum value of 1.96 MPa. In the spillway region, tensile stresses in the downstream face decrease from 6.70 MPa in the case of linear model to a low value of 4.13 MPa for the smeared crack model. However, this decrease is not as significant in the upstream face, i.e. it decreases from 5.90 MPa to 5.68 MPa. The latter is mainly due to the fixed single crack model deficiency and possibilities of high tensile stresses in both the arch and the cantilever directions in this region.
- The extent of cracking and softening is more pronounced for a banded region at the base and abutments in the upstream face of dam and a larger zone starting near the spillway region for the downstream face of the dam.
- Although fixed single smeared crack approach has a significant effect on tensile stresses, it is not capable of bounding all of the tensile stresses by the uniaxial tensile strength of concrete.

REFERENCES

1. Bazant, Z. P., and Oh, B. H. (1983). "Crack band theory for fracture of concrete." *Mat. and Struct.*, 16(94),155-177.
2. de Borst, R., and Nautua, P. (1985). "Non-orthogonal cracks in a smeared finite element model." *Engrg. Computations*, 2(3), 35-46.
3. Cervera, M. (1986). *Nonlinear analysis of reinforced concrete structures using three dimensional and shell finite element models*. PhD dissertation, Dept. of Civil Engrg., Univ. Coll. of Swansea, Wales.
4. Clough, R.W., Chang, K.T., Chen, H.Q., and Ghanaat, Y. (1985). "Dynamic interaction effects in arch dams." Report No. UCB/EERC-85/11 *Univ. of Calif., Berkeley*, Calif.

5. Dowling, M.J., and Hall, J.F. (1989). "Nonlinear seismic analysis of arch dams." *J. Engrg. Mech.*, ASCE, 115(4), 768-789.
6. Espandar, R. (1999). "SNAP - Seismic Nonlinear Analysis Program." *Amirkabir University Software*.
7. Espandar, R., and Lotfi, V. (1999). "Application of a smeared crack model in earthquake analysis of arch dams." Article submitted to *Dam Engrg.*
8. Fenves, G. L., and Mojtahedi, S. (1993). "Earthquake response of an arch dam with contraction joint opening." *Dam Engrg.*, Vol. 4, No. 2.
9. Lotfi, V. (1996). "Comparison of discrete crack and elasto-plastic models in nonlinear dynamic analysis of arch dams." *Dam Engrg.*, Vol. 7, No. 1.
10. O'Connor, J.P.F. (1985). "The modeling of cracks, potential crack surfaces and construction joints in arch dams by curved surface interface elements." *Proc., 15th Int. Conf. on Large Dams*, Lausanne, Switzerland.
11. Rots, J.G. (1988). *Computational modeling of concrete fracture*. Dissertation, Dept. of Civ. Engrg., Delft Univ. of Tech., The Netherlands.

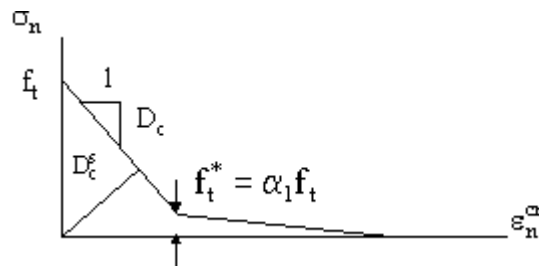


Figure 1: Bilinear idealization of strain softening branch

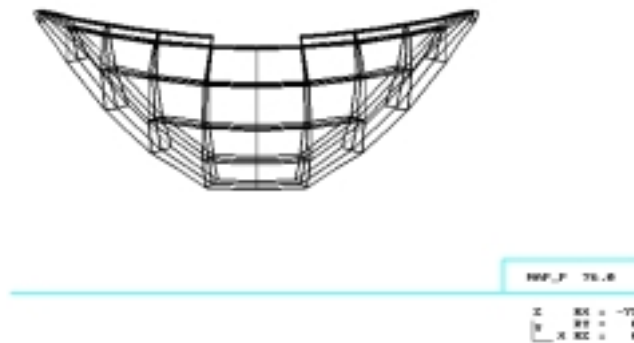


Figure 2: Idealized model of Shahid Rajaee concrete arch dam

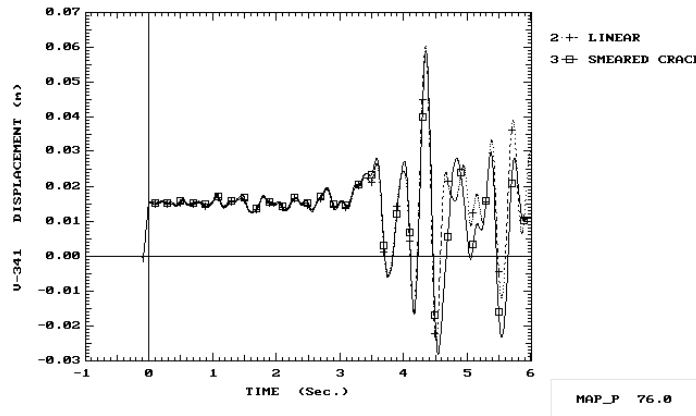


Figure 3: Comparison of displacements in stream direction at quarter points of dam crest between linear and smeared crack models

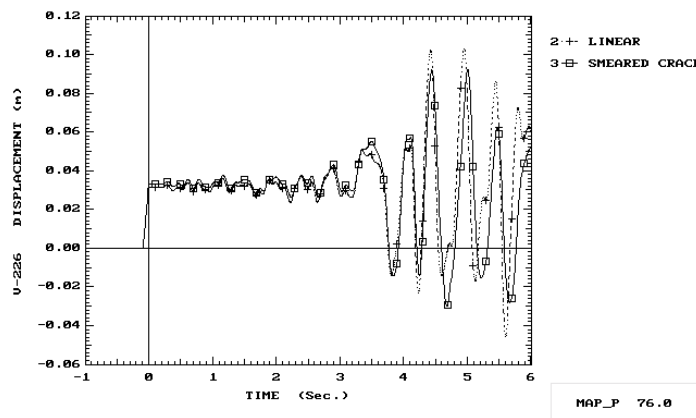


Figure 4: Comparison of displacements in stream direction at center point of dam crest between linear and smeared crack models

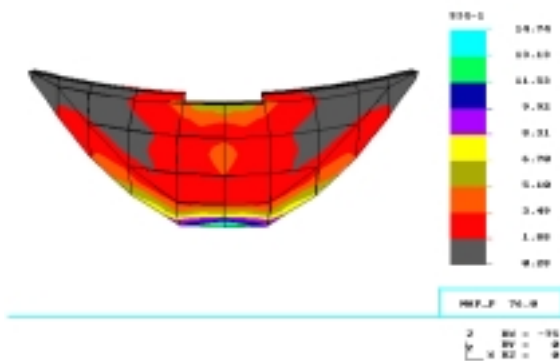


Figure 5: Envelope of max tensile principal stresses (MPa) for linear model (Case L, Upstream View)

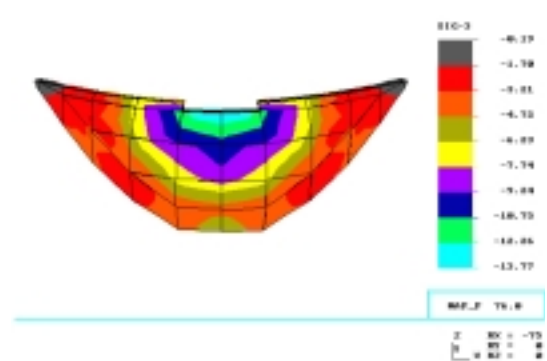


Figure 6: Envelope of max compressive principal stresses (MPa) for linear model (Case L, Upstream View)

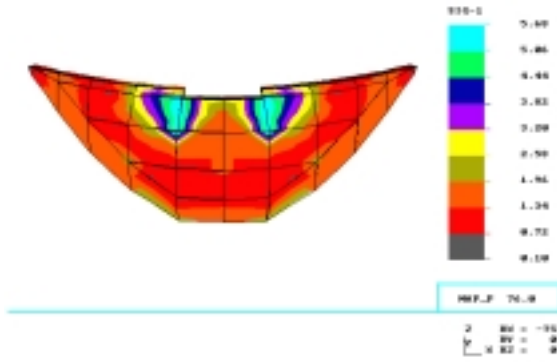


Figure 7: Envelope of max tensile principal stresses (MPa) for smeared crack model (Case SM, Upstream View)

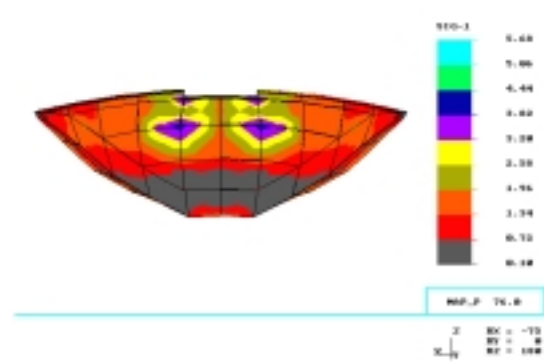


Figure 8: Envelope of max tensile principal stresses (MPa) for smeared crack model (Case SM, Downstream View)

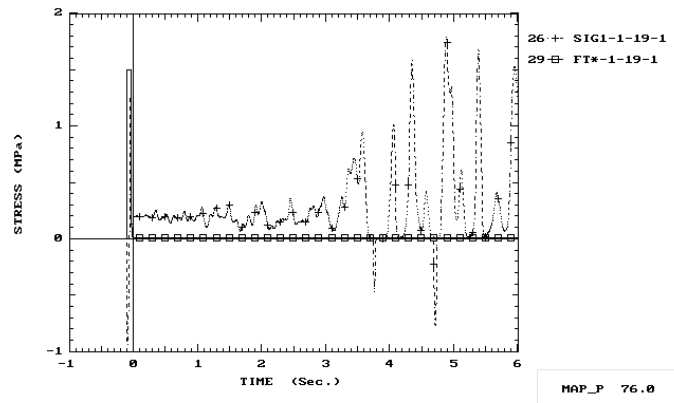


Figure 9: Comparison of max principal stresses and reduced tensile strength (MPa) at base of the dam on upstream face for smeared crack model

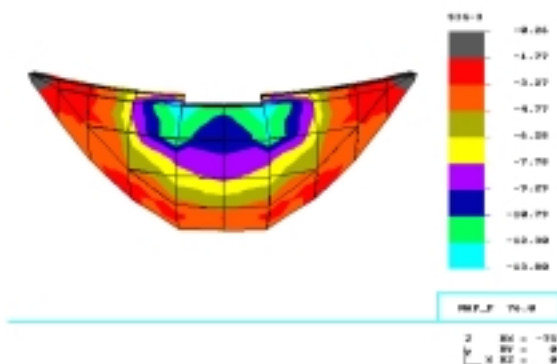


Figure 10: Envelope of max compressive principal stresses (MPa) for smeared crack model (Case SM, Upstream View)

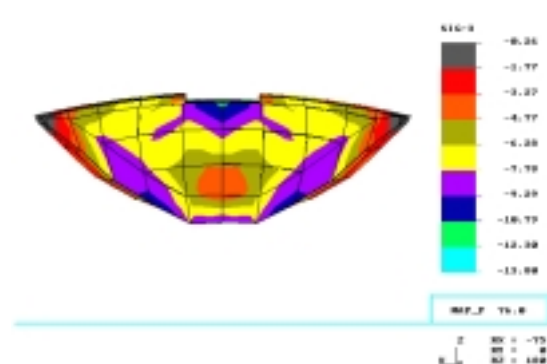


Figure 11: Envelope of max compressive principal stresses (MPa) for smeared crack model (Case SM, Downstream View)

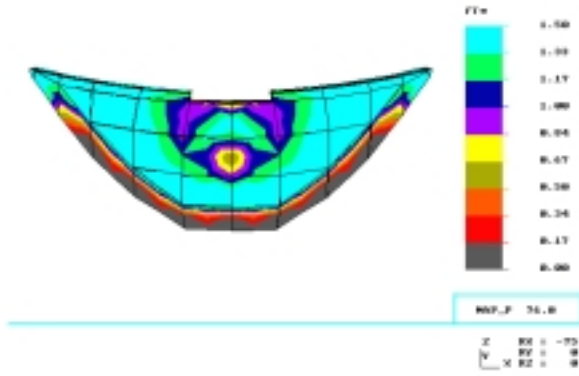


Figure 12: Reduced tensile strength (MPa) at the end of analysis for smeared crack model (Case SM, Upstream View)

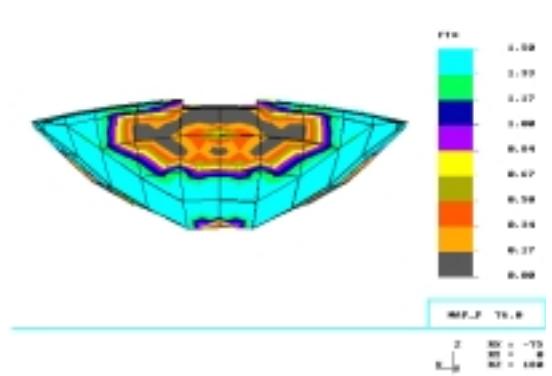


Figure 13: Reduced tensile strength (MPa) at the end of analysis for smeared crack model (Case SM, Downstream View)

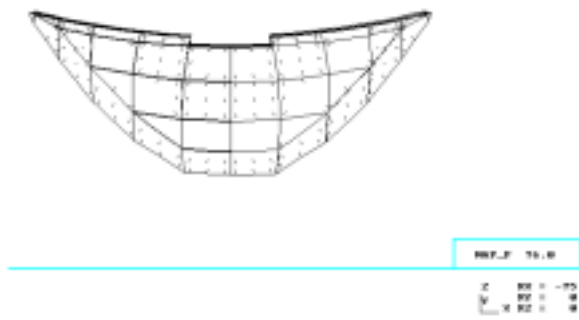


Figure 14: Crack pattern at the end of analysis for smeared crack model (Case SM, Upstream View)

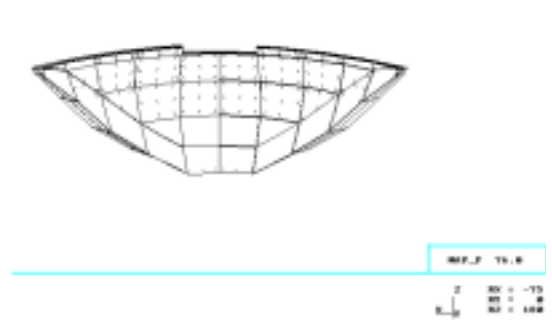


Figure 15: Crack pattern at the end of analysis for smeared crack model (Case SM, Downstream View)